TEM studies of precipitation of metastable phases in 6000 series aluminium alloys

Lidia Lityńska-Dobrzyńska

The alloys of 6000 series (Al-Mg-Si-(Cu)) constitute an important group of alloys designed mainly for applications in the construction, automotive engineering, shipbuilding and aviation industries. They reveal very good plasticity and corrosion resistance and satisfactory strength compared to other heat treatable alloys such as 7000 (Al-Zn-Mg-Cu) and 2000 (Al-Cu-Mg) [1]. The increase in strength is a result of precipitation of different types of metastable phases forming in aluminium solid solution. The understanding and control of precipitation during artificial ageing is therefore critical for achieving optimal properties. Determination of the crystallographic structure of the metastable phases is difficult due to the small size of the precipitates (of the order of several nanometers) and their similar morphology. This makes it necessary to use advanced techniques of transmission electron microscopy (TEM), especially the high resolution microscopy (HRTEM), which allows analysis of individual particles by direct observation of their structure in atomic scale.

It is assumed that the precipitation sequence during ageing in 6000 series aluminium alloys occurs according to the general scheme described for the ternary Al-Mg-Si alloys:

Supersaturated solid solution α(Al) $\Rightarrow$ GP zones $\Rightarrow$ β'' $\Rightarrow$ β' $\Rightarrow$ β (Mg_2Si)

The α(Al) supersaturated solid solution is formed upon rapid cooling from the solution heat-treatment (about 550 °C) to room temperature. The clusters of Mg and Si atoms are formed as coherent with the matrix GP zones at the first stage of decomposition of the α(Al). Next, partially coherent, very fine needles of metastable β'' phase and metastable β' phase in the form of rods, both lying along the <100> direction of the matrix precipitate. The final product of decomposition is the equilibrium β (Mg_2Si) phase.

Most industrial 6000 series aluminium alloys contain small addition of copper which improves the mechanical properties and corrosion of ternary alloys [2-6]. Based on detailed TEM studies a number of additional metastable phases has been identified and it was also shown that the precipitation process is much more complex than described the diagram presented above. The precipitation sequence and type of metastable phases in Al-Mg-Si-Cu alloys depend on the composition, in particular the ratio of Mg to Si and Cu content, as well as the type of heat treatment. Sequence evolution during ageing for different groups of Al-Mg-Si-Cu alloys are shown in Table 1. Three main groups of alloys were taken into account: (1) ternary Al-Mg-Si alloys, in which the ratio of Mg and Si atoms is 2:1 corresponding to Mg_2Si phase, (2) alloys of increased content of Si compare to the Mg_2Si phase and (3) alloys with Cu addition. The phases were assigned to the following aging conditions: initial stage (prior to hardness maximum), peak age (hardness maximum), overage condition and equilibrium stage. In the Table 2 crystallographic data of the phases identified in Al-Mg-Si-Cu alloys, most frequently cited in the literature, are presented [8, 9].

Table 1. Precipitation sequence for different Al-Mg-Si-(Cu) alloy compositions

Alloy composition	Prior peak age	Peak age	Overage	Equilibrium
Al-Mg_2Si	GP zones	β''	β'	β
Al-Mg_2Si+Si	GP zones	β''	β'+B+A+C	β+(Si)
Al-Mg_2Si+Si+Cu	GP zones	β''+QP	β'+QC+Q′	Q+(Si)+(β)+(Θ)

Table 2. Crystallographic data of the phases in Al-Mg-Si-(Cu) alloys

Phase	Structure, lattice parameters	References
GP zone	Orthorhombic; a=0.808 nm, b=0.874 nm, c=0.405 nm	10
GP zone	Face-centered cubic; a=0.405 nm	11
Pre-β″	Monoclinic; a=1.478 nm, b=0.405 nm, c=0.4 nm, β=106.8°	12
β″	Base-centered monoclinic; a=1.534 nm, b=0.405 nm, c=0.683 nm, β=106°	13
β″	Monoclinic; a=0.65 nm, b=0.76 nm, c=0.405 nm, γ=70°	14
β″	Monoclinic; a=0.77 nm, b=0.67 nm, c=0.203 nm, γ=75°	15
β′	Hexagonal; a=0.71 nm, c=0.405 nm,	16, 17, 18
β′	Hexagonal; a=0.407 nm, c=0.405 nm,	19
Type A	Hexagonal; a=0.405 nm, c=0.67 nm	17
U1	Tetragonal; a=0.405 nm, c=0.674 nm	20
Type B	Orthorhombic; a=0.683 nm, b=0.794 nm, c=0.405 nm	17
U2	Orthorhombic; a=0.675 nm, b=0.405 nm, c=0.794 nm	21
Type C	Hexagonal; a=1.04 nm, c=0.405 nm	17
B′	Hexagonal; a=1.04 nm, c=0.405 nm	22, 23
M, Q’	Hexagonal; a=1.04 nm, c=0.405 nm	24, 25, 26
QP	Hexagonal; a=0.395 nm, c=0.405 nm	18
QC	Hexagonal; a=0.71 nm, c=0.405 nm	18
Q-$Al_3Cu_2Mg_9Si_7$	Hexagonal; a=1.039 nm, c=0.402 nm	27
β-Mg_2Si	Cubic; a=0.64 nm	28, 29

Precipitation process begins by forming GP zones from supersaturated α(Al) during ageing below 200 °C for all group of alloys. According [10], GP zones are made of two rows of Mg atoms and one Si, grown on (0-11) planes along the [100] direction and the ratio of Mg/Si is 2/1 in the Al-Mg_2Si alloys. Based on HRTEM studies [11] a model of GP zone in the form of thin plates made of alternating rows of Mg and Si atoms on the (100) planes of the matrix have been proposed. The chemical composition of the GP zones defined as Mg/Si=1 was confirmed in later studies [30]. Another form of precipitates called pre-β″ created by the substitution of Al by Mg and Si atoms [12]. They precede the precipitation of β″ phase and are in the form of few nanometers needles with chemical composition corresponding to $(Al+Mg)_5Si_6$ (because of nanometric dimensions and a high degree of coherence with the matrix they are also considered as GP zones). Spherical GP zone in which the atomic ratio of Mg/Si is close to 1 was observed in alloys with the addition of Cu, wherein the copper atoms are not involved in their forming [31].

In the next stage of aging corresponding the hardness maximum the precipitation of metastable β″ phase occur, which is the main strengthening phase of 6000 series alloys. It is generally accepted that this phase is monoclinic, but there are differences in determination of the crystallographic parameters, which depend on the ratio Mg/Si and the presence of copper

[13, 14, 15]. The β″ phase in the form of fine needles lying along the <001> direction of the matrix has the following crystallographic relationship with the α(Al): (001)β″//(001)α(Al), [100]β″//[310]α(Al) [13, 14, 15]. Precipitates are coherent with the matrix along the direction parallel to the length of needle and partially coherent in the perpendicular direction. Their chemical composition can be estimated as Si:Al:Mg = 6:3:1. As an example, the HRTEM image of β″ phase in the Al-1.0 wt% Mg_2Si-0.4 wt% Si alloy and the proposed scheme of crystallographic structure [15] is presented in Fig. 1. On the basis of HRTEM observation the metastable QP phase have been describe in the alloys containing copper, which replaced β″ phase at peak age. Further aging of the alloy leads to the formation of metastable QC phase, then the equilibrium Q phase [18].

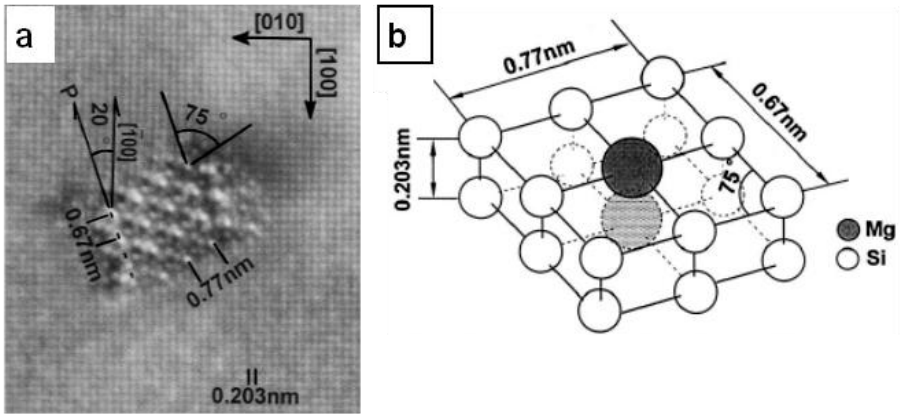

Fig. 1. (a) HRTEM image of the β″ precipitate in Al-1 wt% Mg_2Si-0.4 wt% Si alloy and (b) crystal structure [15]

The β′ is the dominant phase in overaged condition (decrease of hardness) in Al-Mg_2Si alloys and occurs in the form of rods lying along the direction <100> direction of the matrix [16, 17, 18]. The metastable phases described by Matsuda [17] as type A, type B and type C, observed in the alloys with a higher content of Si and corresponding diagrams of crystal structures are shown in Fig. 2. The B-type phase is accompanied often by β′ phase and formed first during aging. Further aging results in the precipitation of the A-type phase and then C-type. Type A and B precipitates are also describes as U1 and U2, respectively [20].

The B′ phase [22, 23], phase M [24] and phase Q′ [25, 26] were identified in alloys containing copper. Crystallographic structure of Q′ phase is analogous to the C-type phase observed in ternary Al-Mg-Si alloys. This phase precipitates in the form of small lath lying along <100> direction of α(Al) and has the following crystallographic relationship to the matrix: (0001)Q′//(001)α(Al), [2-1-10]Q′//<510>α(Al) [24]. TEM bright field image of the 6013 (Al-1.15 wt% Mg-1.1 wt% Si-1.1 wt% Cu) alloy aged for 24 hours at 165 °C (overage) is shown in Fig. 3a [7]. Fine needle-like precipitates uniformly distributed in the matrix were found to lie along <001> direction of α(Al). Close examination of the end-on section of these precipitates (lying parallel the electron beam) revealed rectangle or round shape, characteristic for Q′ and β′ phase, respectively. The corresponding electron diffraction pattern showed reflections within the streaks along the <001> directions (Fig. 3b). The streaks arise from the shape effect of the two variants of the needles lying perpendicular to the electron beam. The schematic simulated diffraction pattern of β′ and Q′ presented in fig. 3c match the maxima on

the streak in the diffraction pattern (Fig. 3b) very well. Detailed study of the Q′ phase by energy-filtered transmission electron microscopy (EFTEM) shown copper segregation at the Q′/(α)-Al interface in an Al-1.0 wt% Mg_2Si-0.5 wt% Cu alloy, what probably limits the diffusional growth of the Q′ phase and produces finer microstructure.

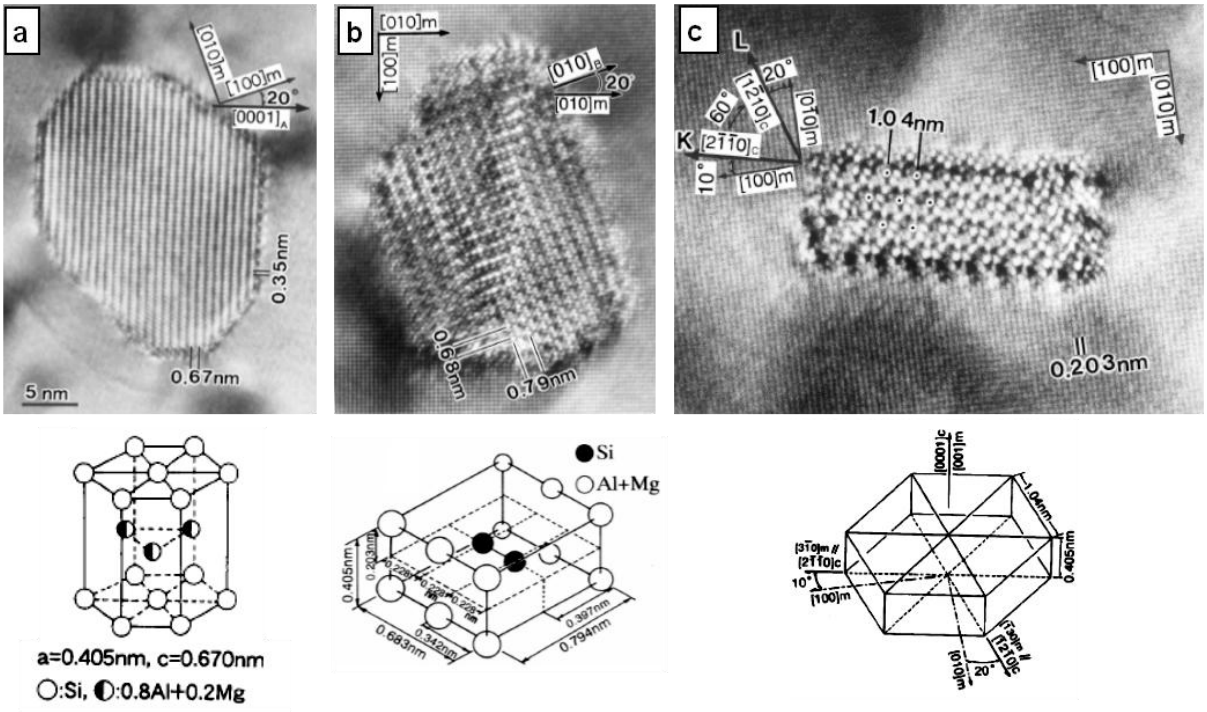

Fig. 2. HRTEM images and crystal structures of the type-A (a), type-B (b) and type-C (c) precipitates in Al-1 wt% Mg_2Si-0.4 wt% Si alloy aged at 525K for 12 ks [17]

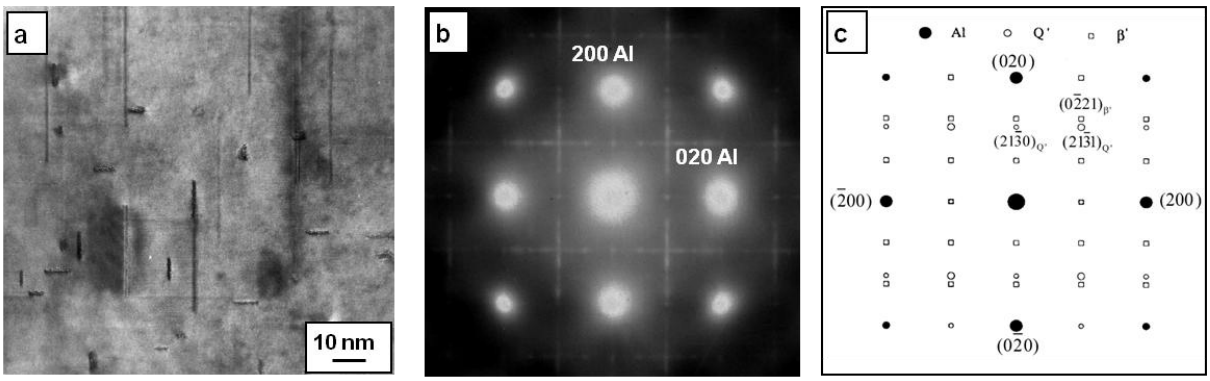

Fig. 3. (a) TEM microstructures of 6013 (Al-1.15 wt% Mg-1.1 wt% Si-1.1 wt%. Cu) alloy aged 24 hours at 165°C; (b) corresponding diffraction pattern – [001] α(Al) zone axis and (c) a simulated diffraction pattern of β′ and Q′ phases in Al matrix.

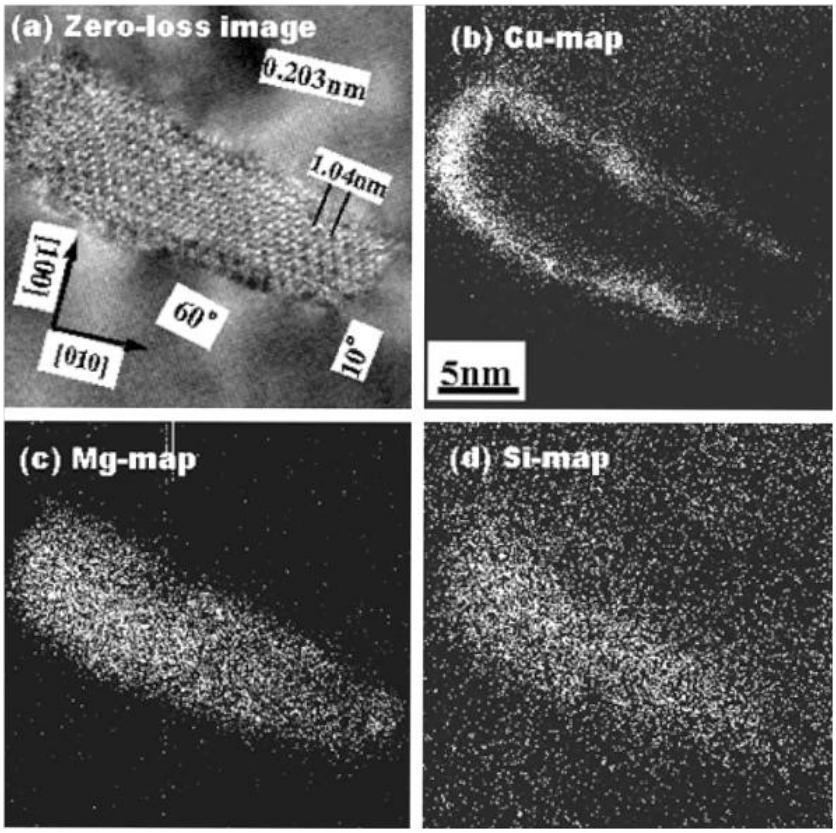

Fig. 4. EFTEM images of the Q′ phase in the Al-1.0 wt% Mg_2Si-0.5 wt% Cu alloy aged at 523 K for 2.4 ks (a) Zero-loss image, (b) Cu-L map, (c) Mg-K map, (d) Si-K map [32]

The only equilibrium phase in Al-Mg_2Si alloys is β (Mg_2Si). In the alloys containing Si excess, Si coexist with β phase, the amount of which increases with increasing silicon content in the alloy [28, 29]. The β phase occurs together with Q, Si and Θ (Al_2Cu) in the alloys containing copper and presence of these phases depends on the relative content of alloying elements. Figure 5 shows the TEM microstructure obtained for Al-1.1 wt% Mg-0.9% wt% Si-1.6 wt% Cu alloy aged 200 h at 165 °C, where the most common particles are the plate shape Θ phase and irregular shape Q phase identified by means of X-ray microanalysis (EDX) and microdiffraction. Both types of precipitates often combine to form a complex conglomerates. Elemental maps of the area visible on the TEM image confirm that the precipitates of the Q phase contain Mg, Cu and Si, while the plate precipitate identified as phase Θ are enriched in copper. Based on the microdiffractions obtained for Q and Θ particles, the following crystallographic relationships can be determined respectively: [0001]Q//[001]Al, (21-30)Q//(100)Al; [010]Θ//[001]Al, [001]Θ//[010]Al.

Figure 6 shows the hardness changes of two alloys with different Cu content: 6013 (Al-1.15 wt% Mg-1.1 wt% Si-1.1 wt% Cu) and 6xxx (Al-1.1 wt% Mg-0.9% wt% Si-1.6 wt% Cu) aged at room and elevated temperature (165 °C and 250 °C) [5, 6]. After quenching the both alloys have similar hardness of about 70 HV. The 6xxx alloy shows higher hardness increase with aging time at all temperatures as compared to 6013 alloy. The maximum value of HV=143 and HV=152 is attained for 6013 and 6xxx alloys respectively, after 8 hours of aging at 165 °C. The hardness increase of the alloy with a higher content of copper is associated with an increased density of the precipitates of metastable phases. Figure 1b, c shows TEM microstructures of 6013 and 6xxx alloys, respectively, aged 8 hours at 165 °C. Fine, uniformly dispersed precipitates in the form of needles lying along <100> direction of

the matrix are visible in both alloys. Two types of precipitates could be recognized among the precipitates located parallel to the [001] direction of the matrix (end-on): a rectangular, of the Q phase and round shaped of β′ phase. A comparison of microstructures shows that density of precipitates increases and their size decreases with increasing Cu content (alloy 6xxx).

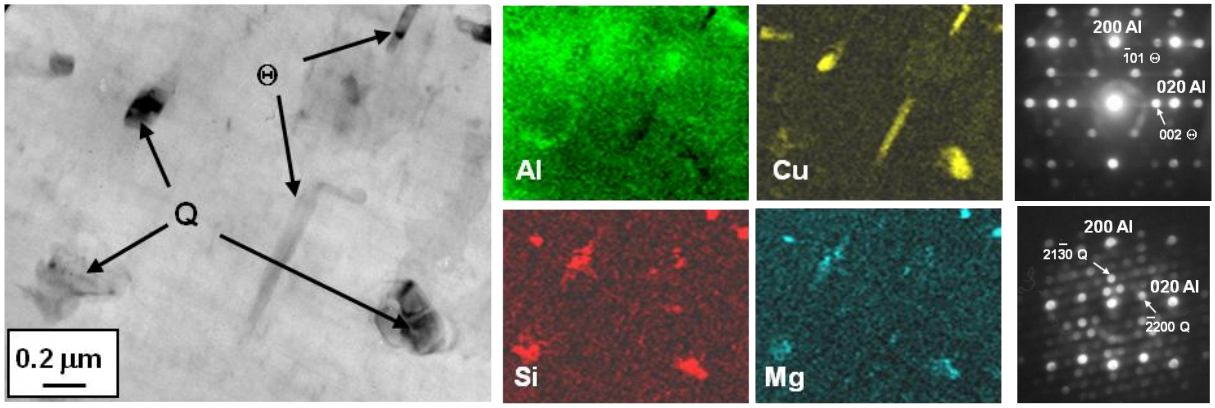

Fig. 5. TEM microstructure of the Al-1.1 wt% Mg-0.9 wt% Si-1.6 wt% Cu alloy aged 200 h at 165 °C; elemental maps of Al, Cu, Mg and Si; microdiffractions obtained for Θ and phase-zone axis [001] α(Al). [7]

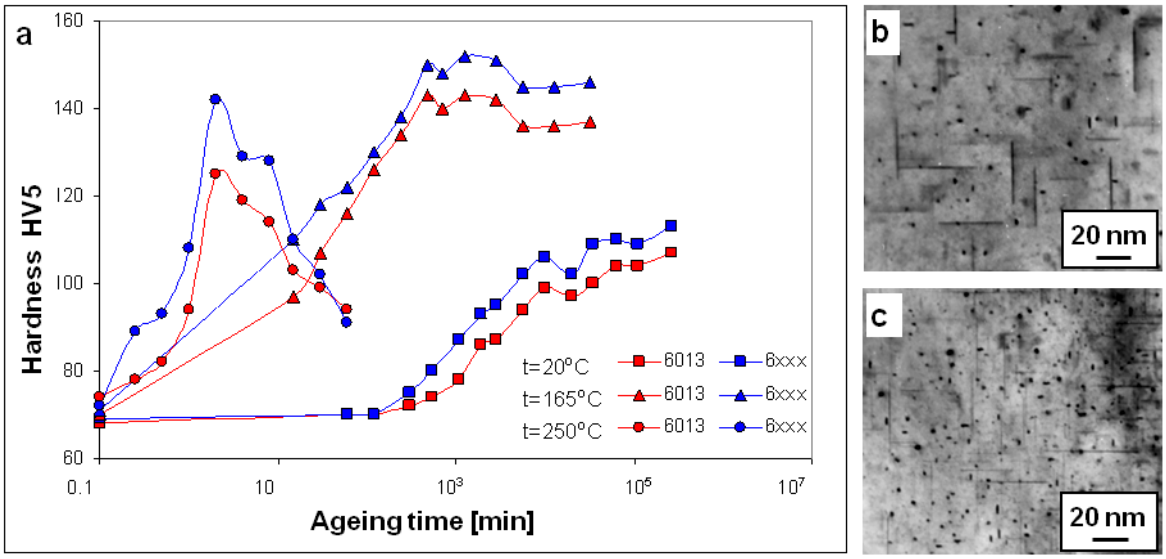

Fig. 6. (a) Hardness changes of 6013 (Al-1.15 wt% Mg-1.1 wt% Si-1.1 wt%. Cu) and 6xxx (Al-1.1 wt% Mg-0.9 wt% Si-1.6 wt% Cu) alloys during aging at room temperature, 165 °C and 250 °C [5]; TEM microstructures of 6013 (a) and 6xxx (b) alloys aged 24 hours at 165 °C – zone axis [001] α(Al) [6]

References:

1. Polmear I.J., Light alloys: from traditional alloys to nanocrystals, Elsevier, 2006
2. Livak R.J., Metall. Trans. 13 A (1982) 1318.
3. Tamizifar M., Lorimer G.M., Proc. of the 3th International Conference on Aluminum Alloys, ed. Arnberg L. et al. NTH Trondheim (1992) 220.

4. Larsen M.H., Walmsley J.C., Lunder O., Nisancioglu K., Mater. Sci. Forum 519-521 (2006) 667.
5. Dutkiewicz J., Morgiel J., Lityńska L., Proc. X Conf. on Electron Microscopy of Solids, Warszawa-Serock, (1999) 187.
6. Dutkiewicz J., Lityńska L., Mater. Sci. Eng. A 324 (2002) 239.
7. Lityńska L., Sholtz R., Dutkiewicz J., Proc. XVII Conf. on Applied Crystallography, Wisła-2000, Ed. H. Morawiec and D. Stróż, World Sci. Publ. Co. Pte. Ltd. (2001) 346.
8. Ravi C., Wolverton C., Acta Mater. 52 (2004) 4213.
9. Chakrabarti D.J., Laughlin D.E., Progress in Mater. Sci. 49 (2004) 389.
10. Thomas G., J. Inst. Metals 90 (1961-2) 57.
11. Matsuda K., Gamada H., Fujii K., Uetani Y., Sato T., Kamio A., Ikeno S., Metal. Mater. Trans. 29A (1998) 1161.
12. Marioara C.D., Andersen S.J., Jansen J., Zandbergen H.W., Acta Mater. 49 (2001) 321.
13. Edwards G.A., Stiller K., Dunlop G.L., Couper M.J., Acta Mater. 46 (1998) 3893.
14. Sagalowicz L., Hug G., Bechet D., Sainfort P., Lapasset G., Proc. of the 4th International Conference on Aluminum Alloys, ed. Sanders T.H. Jr, Starke E.A. Jr, Atlanta, Georgia Institute of Technology (1994) 636.
15. Matsuda K., Naoi T., Fujii K., Uetani Y., Sato T., Kamio A., Ikeno S., Mater. Sci. Eng. A 262 (1999) 232.
16. Jacobs M.H., Phil. Mag. 26 A (1972) 1.
17. Matsuda K., Sakaguchi Y., Miyata Y., Fujii K., Uetani Y., Sato T., Kamio A., Ikeno S., J. Mater. Sci. 35 (2000) 179.
18. Cayron C., Buffat P.A., Acta Mater. 48 (2000) 2639.
19. Matsuda K., Tada S., Ikeno S., Sato T., Kamio A Proc. of the 4th Intern. Conf. on Aluminum Alloys, ed. Sanders T.H., Starke E.A. Jr, Atlanta, Georgia Institute of Technology (1994) 598.
20. Andersen S.J., Marioara C.D., Vissers R., Froseth A.G., Zandbergen H.W., Mater. Sci. Eng. A 444 (2007) 157.
21. Andersen S.J., Marioara C.D., Froseth A.G., Vissers R., Zandbergen H.W., Mater. Sci. Eng. A 390 (2005) 127.
22. Dumolt S.D., Laughlin D.E., Williams J.C., Scr. Metal. 18 (1984) 1347.
23. Edwards G.A., Stiller K., Dunlop G.L., Couper M.J., Acta Mater. 46 (1998) 3893.
24. Sagalowicz L., Lapasset G., Hug G., Phil. Mag. Lett. 74 (1996) 57.
25. Miao W.F., Laughlin D.E., Met. Mater. Trans. 31 A (2000) 361.
26. Matsuda K., Teguri D., Sato T., Ikeno S., Materials Sci. Forum 396-402 (2002) 947.
27. Wolverton C., Acta Mater. 49 (2001) 3129.
28. Matsuda K., Kawabata T., Uetani Y., Sato T., Kamio A., Ikeno S., J. Mater. Sci. 37 (2002) 3375.
29. Ohmori Y., Doan L.C., Matsuura Y., Kobayashi S., Nakai K., Materials Trans. 42 (2001) 2576.
30. Murayama M., Hono K., Acta Mater. 47 (1999) 1537.
31. Murayama M., Hono K., Miao W.F., Laughlin D.E., Met. Mater. Trans., 32 A (2001) 239.
32. Matsuda K., Teguri D., Uetani Y., Sato T., Ikeno S., Scripta Materialia 47 (2002) 833.